New Journal of Physics
The open access journal at the forefront of physics

Deutsche Physikalische Gesellschaft DPG
IOP Institute of Physics

Published in partnership with: Deutsche Physikalische Gesellschaft and the Institute of Physics

OPEN ACCESS

RECEIVED
22 July 2015

REVISED
11 January 2016

ACCEPTED FOR PUBLICATION
1 February 2016

PUBLISHED
19 February 2016

PAPER

Operation of a planar-electrode ion-trap array with adjustable RF electrodes

M Kumph[1], P Holz[2], K Langer[2], M Meraner[2], M Niedermayr[2], M Brownnutt[2,3] and R Blatt[1,2]

[1] Institut für Quantenoptik und Quanteninformation der Österreichischen Akademie der Wissenschaften, Technikerstrasse 21a, A-6020 Innsbruck, Austria
[2] Institut für Experimentalphysik, Universität Innsbruck, Technikerstrasse 25, A-6020 Innsbruck, Austria
[3] Present address: University of Hong Kong, Pok Fu Lam, Hong Kong.

E-mail: muir.kumph@uibk.ac.at

Keywords: ion trap, 2D, radio frequency, array

Supplementary material for this article is available online

Abstract

One path to realizing systems of trapped atomic ions suitable for large-scale quantum computing and simulation is to create a two-dimensional (2D) array of ion traps. Interactions between nearest-neighbouring ions could then be turned on and off by tuning the ions' relative positions and frequencies. We demonstrate and characterize the operation of a planar-electrode ion-trap array. By driving the trap with a network of phase-locked radio-frequency resonators which provide independently variable voltage amplitudes we vary the position and motional frequency of a Ca^+ ion in two-dimensions within the trap array. Work on fabricating a miniaturised form of this 2D trap array is also described, which could ultimately provide a viable architecture for large-scale quantum simulations.

1. Introduction

Trapped atomic ions continue to make advances towards the realization of powerful quantum information processors [1, 2]. There exist several distinct proposals for scaling the current proof-of-principle demonstrations to systems with hundreds or thousands of ionic qubits. These include using a single, anharmonic trap confining a long chain of ions [3]; creating an array of traps through which small groups of ions can be shuttled [4]; and generating an array of separate traps, between which interactions can take place [5, 6]. The latter method of scalability lends itself well to both one-dimensional (1D) and two-dimensional (2D) arrays of ions. 2D arrays could be particularly useful for realizing simulations of 2D systems [7, 8]; for creating entanglement resources for measurement-based quantum computing [9]; and for facilitating robust quantum computation architectures [10].

In pursuing an architecture consisting of a 2D array of trapped ions we consider a scheme in which ions within the array interact with their nearest neighbours. The tunable interaction strengths can be turned on and off using such schemes as proposed by Cirac and Zoller [5] and Bermudez *et al* [6], and successfully implemented in one-dimension to entangle ions in separate wells [11]. In these schemes the time required to implement a gate between a pair of ions (each of mass m and charge q) on resonance scales with the inter-ion separation, a_t, and the ions' motional frequency, ω, as

$$T_{\text{gate}} = \frac{2\epsilon_0 m a_t^3 \omega}{q^2}. \quad (1)$$

Consequently, tuning the interactions requires control over the separation of ions in the two wells, and over the ions' motional frequencies.

Along one axis of a linear trap the ions are confined by static potentials. The relative positions and frequencies of trapped ions along this direction can therefore be tuned by varying DC voltages [12, 13]. By this

means, linear arrays of ion traps have been demonstrated and ions in separate wells have been entangled [11]. The situation in a 2D array of traps, however, is more complicated as the ions are confined in at least two (and possibly three) directions by a pseudopotential created by a radio-frequency (RF) field. Sophisticated efforts to create a 2D array of linear ion traps whereby the ions are shuttled through junctions [4, 14] have constituted an active area of research. Here, a method is investigated to vary the inter-ion spacing in a 2D array of point ion traps [15], while keeping the ions at their respective RF nulls.

There have been experimental demonstrations of confining ions in a 2D array of point ion traps [16]. And the first realization of a 2D array of point traps on a microchip was able to demonstrate the ability to transfer ions between sites [17]. Chiaverini and Lybarger [18, 19] have proposed dynamically re-configurable arrays in which RF electrode 'pixels' could be switched on or off. We have proposed an extension of the basic 2D array architecture by which the RF electrodes are segmented, allowing the positions and frequencies of trapped ions in a 2D array to be tuned by varying RF voltages [15]. As the RF voltage on a particular electrode is reduced, the electric field above that electrode falls, and the ion moves towards the region of reduced electric field. This is then analogous to the tuning of ions' positions and frequencies in a 1D array by varying DC voltages, though it allows the tuning to be done in both directions of the 2D array.

There are a number of methods which may be used to apply RF voltages of different amplitudes to different electrodes, and thereby control the position of the RF null. At low frequencies, dust traps holding lycopodium spores have been reconfigured using variable alternating voltages of 50 Hz [15]. In ion traps, different electrodes can be driven with different amplitude voltages by utilizing different tapping points in a single helical resonator [20]. The RF null has also been moved in a more smoothly continuous fashion by selectively adjusting the load capacitance of the trap electrodes [21, 22]. This latter method has been used to switch between trapping configurations in which ions were in a single linear pseudopotential minimum and in two separated linear traps [23].

Variation of the capacitive load can result in different RF electrodes having different phases, leading to significant micromotion. The method used in the present work is able to vary the amplitude of the RF while actively keeping the RF phase constant by feeding back to a varactor diode. This allows the RF minimum to be significantly displaced within microseconds, while ensuring that there is minimal phase-induced excess micromotion. We implement a system of multiple low-power RF drives with actively locked phase, for which the voltage amplitudes can be independently varied in real time. These are used to trap single $^{40}Ca^{+}$ ions and vary the ion's position in two-dimensions within a 2D array of traps, as well as varying its motional frequency.

The trap-fabrication technology chosen to highlight this variable RF ion control is that of a printed circuit board (PCB) ion trap [24, 25]. While this technology is unlikely to allow high-fidelity quantum operations in ion traps, the ease of fabrication permitted the initial demonstration and testing of the RF displacement method presented here. A more advanced thin-film fabrication technology which might allow high-fidelity quantum operations is described at the end of this paper.

This paper is arranged as follows. First, the trap apparatus, including the associated driving electronics, is described in section 2. The theory underlying a quantitative description of the RF displacement method is presented in section 3. Trapping results, including the variation of an ion's position and motional frequency as a function of the addressable RF voltage, are reported in section 4. To realize a large-scale quantum information processor, the building blocks demonstrated here must be implemented in a system with $\gtrsim$100 ions and $\lesssim$100 μm inter-well separation; section 5 discusses a possible path to realizing such a system.

2. Setup

The apparatus used for the demonstration of controllably varying a trapped atomic ion's position and motional frequency within a 2D array of traps has two distinct aspects to consider: the trap array and the drive electronics. A new trap array was fabricated using PCB technology. This fabrication method is simple and reliable, but limits the trap dimensions to be larger than those required for coherent quantum operations. Importantly, however, it permits for the first time the demonstration of the variable RF drive electronics, operating in a parameter regime congruent with scalable trapped-ion quantum computing. The setup of the trap (including the attendant mounting and vacuum system) and the driving electronics are discussed here in turn.

2.1. Ion-trap array

Following a tradition of naming traps after famous prisons, the trap array design considered here is dubbed '*Folsom*'. The trap array's electrode structure is shown in figure 1. There are 16 circular trapping-site electrodes, each of which is held at RF ground. Above each of these a pseudopotential minimum is formed, 400 μm above the trap surface, which serves to confine ions in all three dimensions, The principal axes of the ions' motion are aligned along the x, y, and z directions shown in figure 1. From symmetry considerations, motion in the xy plane

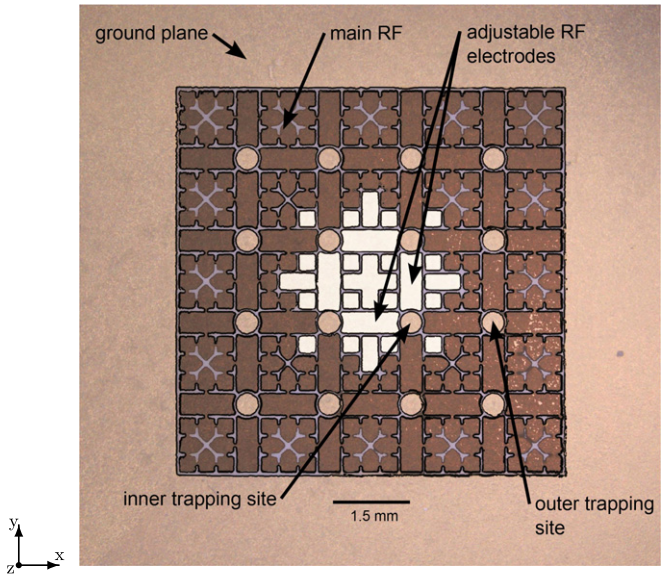

Figure 1. False-colour image of Folsom. Circular trapping-site electrodes are held at RF ground, and ions can be trapped 400 μm above each of these. The outer 12 trapping-site electrodes are connected to DC ground, while the inner four sites have separate connections to allow non-zero DC voltages to be applied. The large square outer electrode is held at ground. There are two types of RF electrodes: the main RF electrode (darkened in figure) forms a single electrode and allows trapping at the outer 12 trapping sites. The inner RF electrodes (lightened in figure) are connected individually to allow independent adjustment of the RF voltages applied. All electrodes are connected by vias to traces on the backside of the printed circuit board. Experiments were carried out first at an outer trapping site and then in a different array at an inner trapping site.

is termed radial motion, and that in the z direction is termed axial motion. Between the trapping-site electrodes of the inner 2 $\times$ 2 array there are individually adjustable RF electrodes. These allow the separation and motional frequency of nearest-neighbouring ions to be reduced, as is required for tunable interactions (see equation (1)). The size of the electrode features is set by the fabrication method used. The resulting trap separation of 1.5 mm is too large to allow coherent quantum operations between the trapping sites [15]. Nonetheless, the structures are sufficiently small to permit a demonstration of the electronic control needed for future, smaller trap arrays. The outer 12 trapping-site electrodes are surrounded by a single planar RF electrode. While their potentials cannot be individually adjusted, the outer sites provide realistic boundary conditions for the inner sites, which will ultimately need to form part of a larger array. A ground plane provides the final electrode needed to generate an RF quadrupole trap. An additional far-field ground is provided by a transparent ground plane (shown in figure 2(d)) mounted 7 mm from the plane of the trap. This has the effect of increasing the trap depth and shielding the trap from stray fields. In the present design this plane is grounded though, if necessary, a DC connection could be made so that it provides a uniform static field, such as may be of use for micromotion compensation.

The steps for Folsom's assembly are shown in figure 2. The electrode structure was etched[4] into the 18 μm thick copper cladding of a PCB[5]. The copper was subsequently plated with 10 μm of gold using a gold sulphite solution[6]. The trap after gold plating is shown in figure 2(a), with the surface detail shown in figure 2(b). The board was then mounted to a 1.6 mm thick substrate using pins[7] which were crimped into vias in the PCB, shown in figure 2(c). This served both to support the PCB and to connectorize it. The connectorized trap and a ground plane[8] were mounted on a custom-made PCB filter board, which was in turn plugged into a cable breakout board. The completed trap assembly is shown in figure 2(d). Coaxial cables from the breakout board were connected to the coaxial feedthrough described below.

The vacuum configuration for the experiment is shown in figure 3. The trap chip was held in an octagonal vacuum chamber at a pressure of 10^{-10} mbar with the trap surface oriented horizontally and facing downwards. The chamber had coaxial feedthroughs mounted to the top flange which provided electrical connections from the RF electronics to the individual trap electrodes. A viewport on the bottom flange allowed imaging of the ions

[4] Fabrication by Andus Electronic GmbH.

[5] Rogers 4350b substrate (35 mm $\times$ 35 mm $\times$ 170 μm).

[6] Transene TSG-250.

[7] Mill-Max 3116.

[8] Indium tin oxide (70–100 $\Omega/\square$) on a fused-silica substrate (25 mm $\times$ 25 mm $\times$ 1 mm).

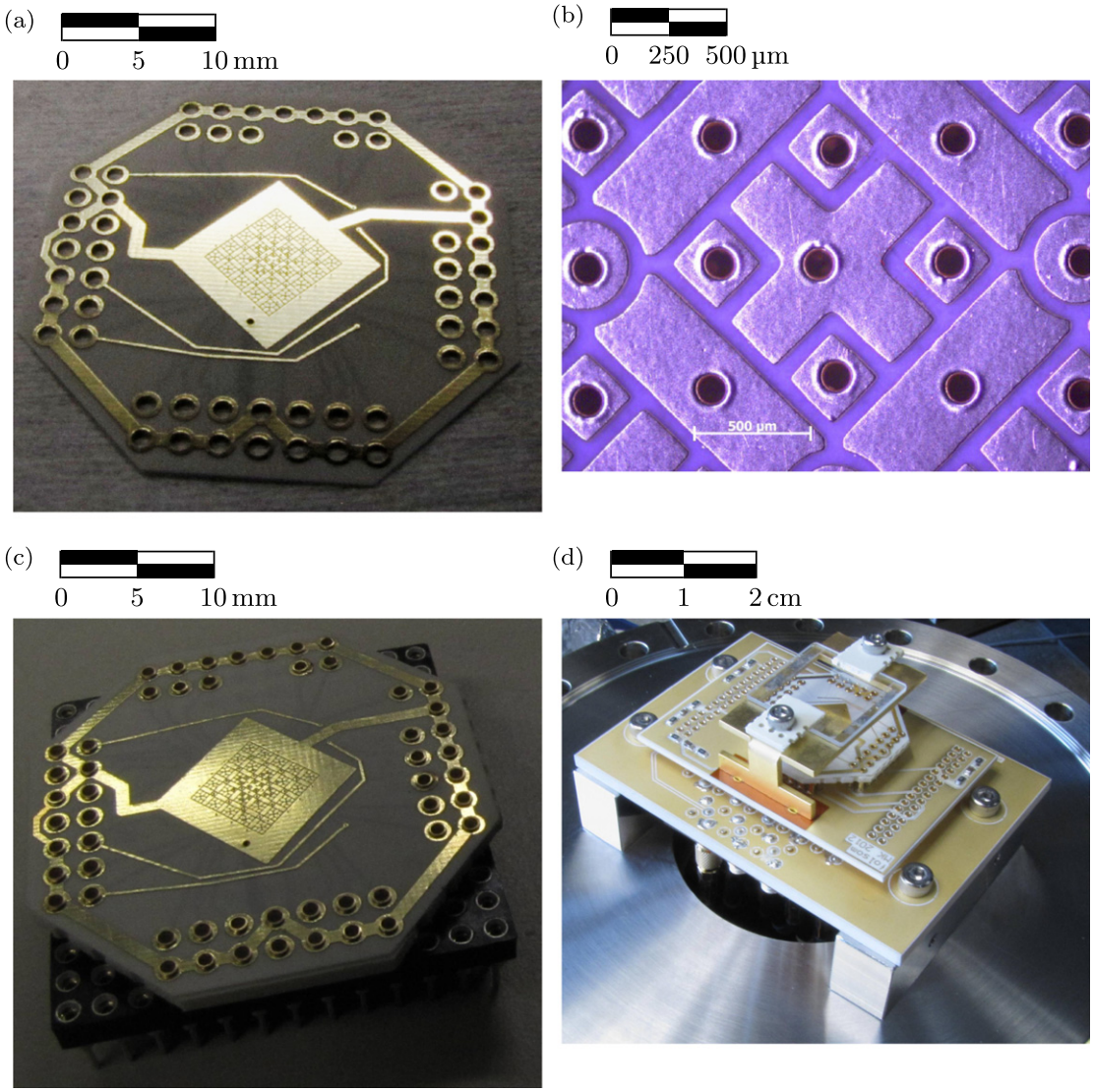

Figure 2. Fabrication and mounting of the ion trap array. (a) Printed circuit board after plating with gold. (b) Detail of the centre electrodes' structure. The black circles are holes where vias connect the electrodes to the backside of the PCB. (c) Connectorized trap. Electrical connections from the trap to the socket are made with pins crimped to the vias at the edge of the PCB. (d) Trap mounted on an in-vacuum filter board and cable breakout board. A clear conductive window is mounted 7 mm from the trap surface. When the entire assembly is installed in the vacuum chamber the trap faces downwards.

onto a CCD camera (not shown in the figure) by a custom objective. The viewports on the sides of the vacuum chamber provided laser access in the plane of the trap array. The ions were cooled and imaged with laser light of wavelength 397 and 866 nm [26].

2.2. Variable RF sources

Controlling the position and motional frequencies of a specific ion within an array requires the relative amplitudes of the RF voltages on adjacent electrodes to be varied. Any relative phase between the voltages on different electrodes, however, will cause the ion to undergo excess micromotion [21, 27], and so it is required that all RF voltages remain in phase. To this end a novel RF drive was developed [28], a simplified schematic of which, is shown in figure 4. In essence, the drive uses a tank resonator to match the impedance of the trap electrode and wiring to that of the RF source, while also using a control circuit to lock the phase of the RF drive's output to a reference. Each RF electrode is then individually driven by such an independently phase-locked RF drive.

When the voltage amplitudes on different electrodes are varied, the capacitance, C_T, of a particular trap electrode to ground may also change. The control circuit shown in figure 4 compares the output voltage of the resonator to a phase reference and adjusts the capacitance of the varactor diode to compensate for any changes in C_T. The tank resonator itself is formed by an inductor, L, and the capacitors shown inside the dashed box in figure 4. The variable capacitor, C_1, allows the frequency of the resonator to be tuned. Capacitors C_2 and C_3 form

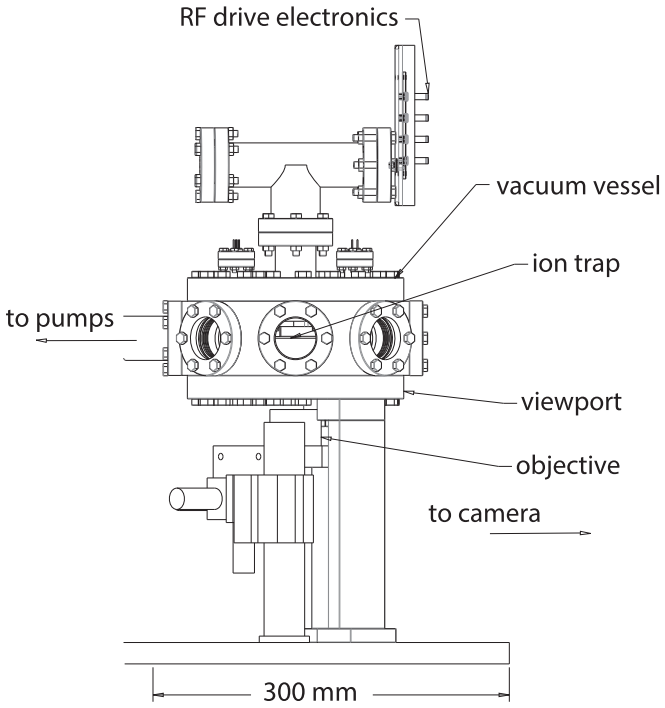

Figure 3. Vacuum setup for testing Folsom. RF feedthroughs at the top allow the trap to be driven by the RF electronics. Imaging of the ions is done through a viewport on the bottom of the vacuum vessel, through an objective. Lasers for cooling and photoionization have access through the viewports on the sides of the vacuum vessel.

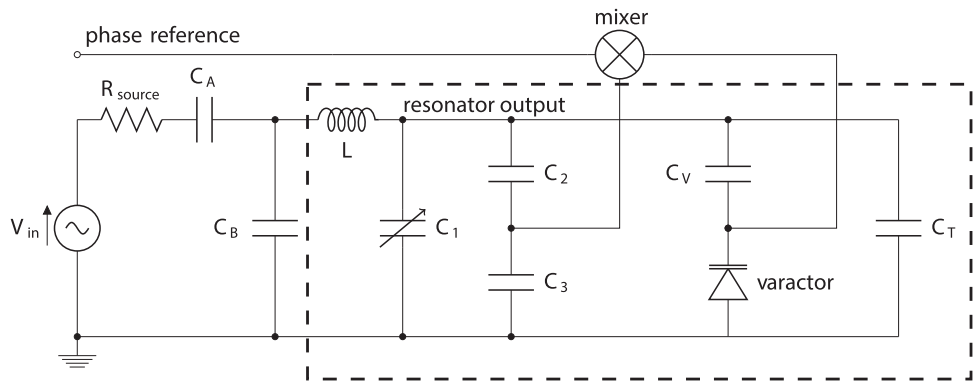

Figure 4. Schematic of the phase-locked RF resonator. A tank resonator is formed by the high-quality inductor, L, and the capacitors shown inside the dashed box. The mixer locks the output phase of the resonator to a phase reference by varying the capacitance of the varactor diode.

a voltage divider to provide a low-voltage pick-off which has the phase of the RF drive's output. Capacitor C_V protects the varactor diode from the RF drive's high output voltage. The capacitors C_A and C_B match the impedance of the tank resonator to the 50 Ω RF source.

Table 1 provides a list of the parts shown in figure 4. The electronic components which are part of the high-voltage resonator (inside the dashed box in figure 4) are selected to have low losses. This allows the high-voltage resonator to maintain a high Q, and hence a high voltage gain. The varactor shown in figure 4 is composed of an array of 32 BB640 varactor diodes in a 2×16 arrangement. This allows a large capacitance variation of 26–280 pF with a control voltage of 5–25 V. To minimize distortion of the output RF waveform relative to the input waveform despite nonlinearities in the varactor behaviour, the two banks of 16 varactor diodes are used opposite to each other in a mirrored configuration. This also allows twice the applied RF voltage to be applied to the varactor array without breakdown. This, in turn, permits a protection capacitor with a larger capacitance C_V to be used, with an associated increase in the dynamic range of the phase lock. The capacitor C_A in figure 4 is composed of two physical capacitors: a fixed capacitor and a trimmer capacitor so as to maximize the match of the resonator to the 50 Ω source impedance. While figure 4 shows the the most significant functional elements,

Table 1. Part list of the circuit in figure 4. The Identifier corresponds to the items in the schematic. The Part number refers to the manufacturer's part number listing.

Identifier	Description and manufacturer	Part number
Varactor	32× Infineon	BB640
C_V, C_2	1.5–5.5 pF Sprague-Goodman Var. Capacitor	GXE5R000
L	10–14 turns 1 mm wire, Micrometals Core	T-50-2
C_1	5–45 pF Sprague-Goodman Var. Capacitor	GXE45000
C_3, C_B	820 pF AVX Capacitor	SQCBEM821KAJME
mixer	Analog Devices	AD8302
C_A	40–100 pF AVX Capacitor	SQCB Series
	12–100 pF Johanson Mfg. Var. Capacitor	9328

the circuit actually used has 94 components. Details of the complete circuit schematic and parts list can be found in the supplementary material available at stacks.iop.org/njp/18/023047/mmedia.

2.3. Adjustment and setup of the variable RF sources

In the experiments described below, the voltages on two (of a possible 25) RF electrodes are independently varied. These electrodes have only a light capacitive load (30 pF) and require the phase to be actively locked in order to keep the phase-walk below $\sim 1^\circ$. The remaining RF electrodes are bundled into groups and driven by three separate RF resonators, which are adjusted to have the same phase. The total capacitive load on each of these resonators is around 200 pF, meaning that the relative changes in the load due to mutual capacitance are sufficiently small to obviate the need to lock their phases.

Correct adjustment of the system requires that the source (V_{in}) has the correct phase and amplitude, that the resonator has the correct resonant frequency (set by C_1), and that the source and resonator are impedance matched (set by C_A and C_B). To achieve this the RF electrodes are all initially set to have nominally the same voltage amplitude, frequency and phase. In this 'home' configuration the optimal conditions are met when the RF power reflected from each of the tank resonators (measured using directional couplers) is minimized.

Changing an ion's position and motional frequency requires the amplitude of one of the RF voltages to be reduced, without altering its frequency or phase. Under such circumstances some amount of RF power is coupled capacitively between RF electrodes with different voltage amplitudes, causing power to be transmitted back up the line, through the resonator, to the RF source. For this reason the method of minimizing the signal through a directional coupler cannot be used away from the home settings to check that the circuit is operating as it should. Instead, an oscilloscope with capacitive-pickup probes is used as an out-of-loop diagnostic to monitor the output phase and amplitude of each RF drive.

3. Theoretical analysis of RF variation

Ion-trap work to date has generally used a single RF source to drive all RF electrodes, though a number of experiments have applied differing RF voltages to each RF electrode to adjust the height of the ion above a surface electrode point trap [20, 22, 29] or adjust the nodal line of RF in linear quadrupole ion traps [21]. Adjustable RF voltages have also been used to convert two neighbouring planar-electrode linear traps into a single linear trap [23]. The distance by which the RF null moves as a function of the relative RF voltages must, in general, be numerically calculated for each trap geometry. Here we present a first-order perturbative approach [28] which permits an intuitively clear, and quantitative treatment of the displacement of the RF null. The method can be applied to a range of applications in which the relative amplitudes of RF voltages are varied, provided the regime of operation is far from having two distinct trapping potentials merge. A more general approach using adjustable quartic potentials [30] allows consideration of the regime in which neighbouring traps merge, though the resulting equations provide a less intuitive picture.

In this section the quantitative effects of adjustable RF electrodes are considered, as well as how these effects can be used to perform RF displacement. First, the effect of an RF voltage applied to a single electrode in a simple trap geometry is considered (section 3.1). RF displacement due to selectively varying the RF voltage amplitude is

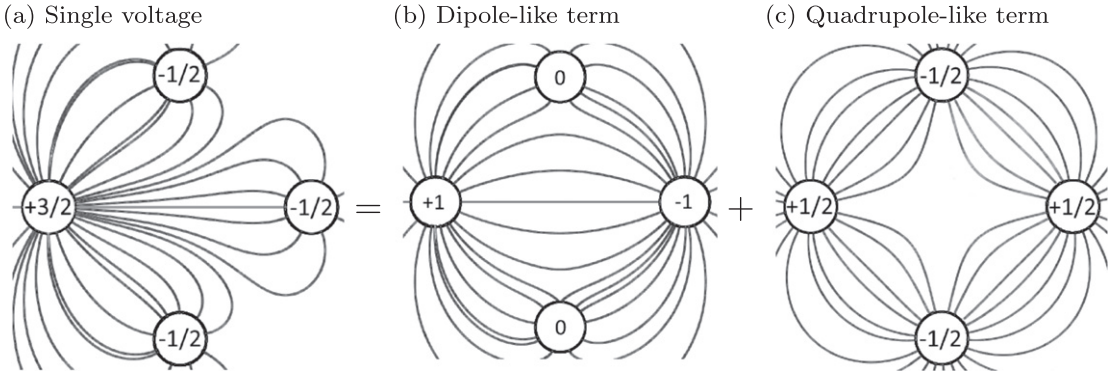

Figure 5. Decomposition of the field due to a voltage on a single trap electrode (a) into a dipole-like term (b) and a quadrupole-like term (c).

described for a 3D trap in section 3.2, and for a surface trap in section 3.3. Quantitative results for the surface-trap geometry demonstrated experimentally in this work are presented in section 3.4.

3.1. Electric field due to a voltage on a single electrode

Consider the electric field due to a voltage on a single electrode in a simple trap configuration. Figure 5(a) shows a trap in a 2D space with four circular electrodes, such as could describe the cross-section of a linear ion trap. The relative voltage on the left electrode is $+2$ V. For reasons of clarity for the following analysis, this voltage difference is shown as $3/2$ V applied to the left electrode and $-1/2$ V to the other three electrodes.

In order to obtain an expression for how the position of the RF null can be moved as a function of the relative voltages on the electrodes, the electric field due to a voltage on a single electrode can be decomposed into a dipole-like (antisymmetric) term and a quadrupole-like (symmetric) term, as shown in figure 5. The electric field arising from the dipole-like term is approximately constant near the geometric centre of the trap (i.e. at $x = 0$). The electric field arising from the quadrupole-like term is zero at $x = 0$ and is, to first order, proportional to $-x$. The x-component of the electric field along the x-axis of the trap can therefore be written as a function of the x position and the voltage, V, on the left electrode as,

$$E_x = V\,[a(x) - xb(x)/2], \tag{2}$$

where a is the zeroth-order electric-field coefficient due to the dipole-like configuration and b is the first-order coefficient (positively defined) of the quadrupole-like configuration. The coefficients a, b are geometry dependent and may be direction dependent, giving rise in the general case to coefficients a_i, b_i for $i \in x, y, z$. Coefficients for a particular geometry and direction can be found by numerical simulation of the trap.

3.2. RF variation in a linear trap

Under the assumption that the phase on all RF electrodes is the same, the location of the RF null (i.e. the trap location) can be computed by considering the electric-field contributions due to an RF voltage on the left (V_1) and right (V_2) electrodes, in terms of the coefficients a and b. The RF null is located at the point where the total electric field is zero, namely

$$x_t = 2\frac{a}{b}\frac{V_1 - V_2}{V_1 + V_2}. \tag{3}$$

If $V_1 = V_2$, then the trap is operating like a normal linear quadrupole ion trap and the trap location is at $x = 0$. Otherwise the RF null is displaced from the geometrical centre of the trap.

The relationship between the applied RF voltages, V_1, V_2, and the motional frequency of the ion, ω, can be calculated in similar fashion, and can be shown to be

$$\omega = \frac{q|b|}{\sqrt{8}\,m\Omega_{RF}}(V_1 + V_2), \tag{4}$$

where Ω_{RF} is the frequency of the RF source.

3.3. RF variation in a simple surface trap

The principles outlined above can be readily extended to planar structures. By calculating, for a particular geometry, the values of the coefficients a and b, and provided the displacement from the trap centre is sufficiently

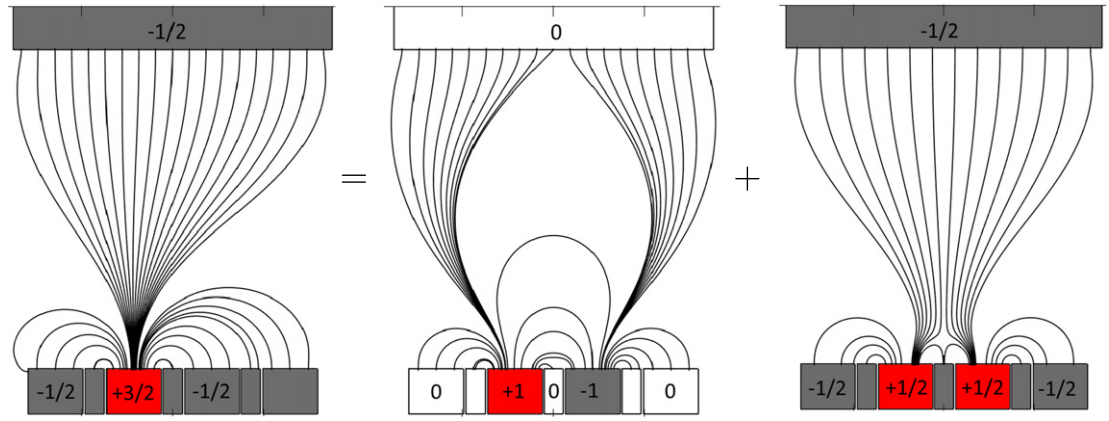

Figure 6. Decomposition of the field due to a single voltage in an array of surface ion traps (a) into a dipole-like field (b) and a quadrupole-like field (c). The electrode above the trap is a ground plane, which is often used in surface trap experiments to shield the trap from stray fields and to increase the trap depth. Experiments described in this paper have such a ground plane, though the principles of decomposing fields into dipole-like and quadrupole-like components do not require it.

small that these coefficients can be considered constant, equation (3) can be used to estimate the RF displacement and equation (4) can be used to estimate the motional frequency, ω.

Such a decomposition can be illustrated by considering a 3×1 array of surface-electrode ion traps. Figure 6 shows the decomposition of the field due to a voltage on just one addressable RF electrode (figure 6(a)) into a dipole-like field (figure 6(b)) and a quadrupole-like field (figure 6(c)). The location of the quadrupole RF null (i.e. the home position of the trap) is above the middle trap electrode (see figure 6(c)). Although the geometry here is significantly different from the linear-trap geometry considered in sections 3.1 and 3.2, the fields can be decomposed in the same way.

3.4. RF displacement in Folsom

The method described above to quantify the displacement of the ion in a geometry with just a few RF electrodes can be generalized to geometries with many more adjustable RF electrodes, such as Folsom. In such a case, the extra RF fields from the other electrodes must also be taken into account. Figure 7 shows the electrode structure of the Folsom array. The electrodes RF1, RF2, and G1 are the relevant electrodes for computing the dipole and quadrupole coefficients around the trap position above electrode G1. The residual RF field from the rest of the RF electrodes (coloured red), must also be taken into account.

The dipole-like and quadrupole-like coefficients are calculated for the adjustable RF electrodes (RF1 and RF2) on either side of a trapping-site electrode (electrode G1) by numerical simulation of the full trap geometry. The electric field near the home trapping position, due to voltages V_1 and V_2 on the adjustable electrodes RF1 and RF2 is

$$E_{\mathrm{Adj}} = V_1(a - bx/2) - V_2(a + bx/2). \tag{5}$$

As the trapping site is located in an array which contains periodic even symmetry of the RF electrodes, the RF voltage, V_{A}, on all the other RF electrodes creates a weak quadrupole field at the centre of the trapping site. This additional field E_{A} can be parametrized as

$$E_{\mathrm{A}} = -V_{\mathrm{A}} cx/2, \tag{6}$$

where c is the positively defined quadrupole-like coefficient of the rest of the array's electrodes, and x is the distance from the centre of the trapping site of interest. The RF null is located at the point where the total field, $E_{\mathrm{Adj}} + E_{\mathrm{A}}$, is zero:

$$x_{\mathrm{t}} = 2\frac{a(V_1 - V_2)}{b(V_1 + V_2) + cV_{\mathrm{A}}}. \tag{7}$$

Again, the relationship between the applied RF voltages, V_1, V_2, V_{A}, and the motional frequency of the ion, ω, can be calculated in similar fashion, and can be shown to be

$$\omega = \frac{q}{\sqrt{8}\, m\Omega_{\mathrm{RF}}}\{|b(V_1 + V_2) + cV_{\mathrm{a}}|\}. \tag{8}$$

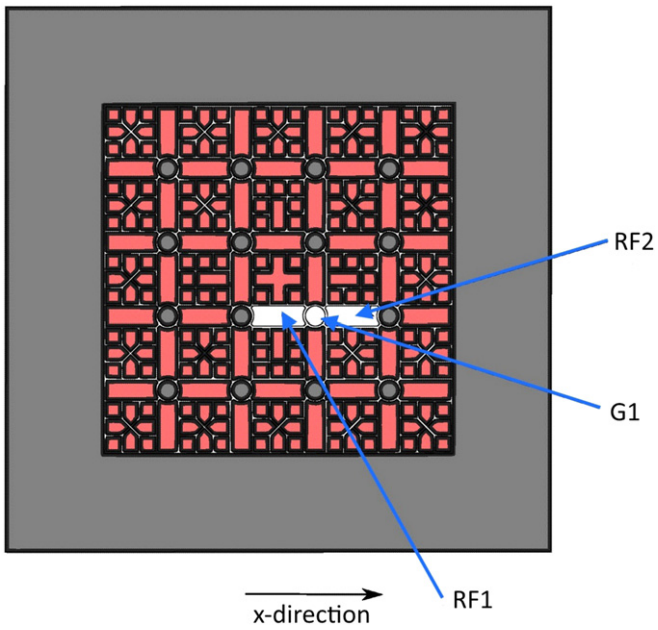

Figure 7. Setup for simulating the effect of RF variation in the Folsom trap array. The adjustable RF electrodes RF1, RF2, and trapping-site electrode G1 are used to calculate the dipole and quadrupole coefficients. The effect of the RF field from the rest of the RF electrodes (coloured red) can be considered as an additional quadrupole perturbation.

Numerical simulations of the Folsom array provide the values $a = 500\ \mathrm{m}^{-1}$, $b = 3.0 \times 10^6\ \mathrm{m}^{-2}$, $c = -1.4 \times 10^5\ \mathrm{m}^{-2}$. Assuming that $V_2 = V_A$, it can be seen from equation (7) that a reduction of 4 dB (i.e. around 37%) in the RF voltage applied to electrode RF1 would lead to a displacement of the RF null by 77 μm. According to equation (8), the same change in V_1 would lead to a ~19% reduction in the ion's motional frequency.

4. Results

The operation of the Folsom array is described here. This section first presents the trapping of single ions at one of the outer 12 trapping sites of the array using a single RF source and ground. Secondly, trap operation at one of the inner 4 trapping sites using multiple phase-locked RF sources is presented. At the inner site the voltages on specific RF electrodes can be individually and independently adjusted to demonstrate control over both the ion's position and its motional frequency in two-dimensions. Finally, heating-rate measurements made at the outer and the inner trapping sites are presented.

4.1. Ion trapping

Single $^{40}Ca^+$ ions were loaded at one of the outer trapping sites (indicated in figure 1) using a single RF trap drive connected to the main RF electrode. The ion's secular motional frequency in the z direction (normal to the trap surface) was measured to be 680 kHz at a trap-drive frequency of 10.7 MHz and an RF voltage amplitude of 100 V (0 pk). The lifetime of a single ion with the cooling lasers on was approximately 10 min.

The trapping behaviour at the outer trapping site deteriorated over time, with increased difficulty in loading, increased micromotion, and decreased trapping lifetimes. Possible reasons for this behaviour are discussed below. After several months of such deterioration it was no longer possible to load ions. A new trap array (of the same design) was then installed and used for all subsequent experiments described in this paper.

In the new trap array, single $^{40}Ca^+$ ions were loaded at one of the inner trapping sites (indicated in figure 1). For this, multiple RF drives were used to apply RF voltages of the same phase but independently variable amplitudes (see section 2) to the various adjustable RF electrodes. Several of the segmented RF electrodes were connected together, so that five separate RF drives were used to drive the electrodes surrounding the trapping site. Despite the increased complexity of the drive electronics the inner trapping site in this array exhibited similar uncooled lifetimes to the outer trapping site in the first trap array tested.

The home configuration of the multiple RF drives was set such that all of the RF electrodes had the same RF voltage amplitude and phase, mimicking one single, unsegmented RF electrode. The RF drive voltage had an amplitude of 100 V and a frequency of 10.1 MHz. The voltage at the individual electrodes was then varied by

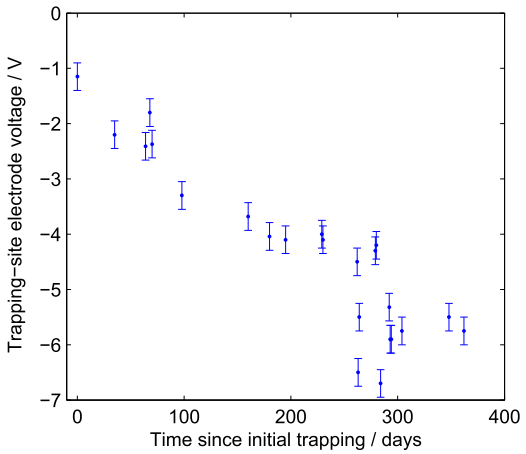

Figure 8. The DC voltage that had to be applied to the trapping-site electrode to allow stable trapping. This became more strongly negative over the course of a year, until it was no longer possible to trap ions.

changing the power applied to the relevant RF resonator. All RF power data below is given in dB relative to the above-specified home configuration.

Trapping ions in the second trap array required that the trapping-site electrode beneath the ion be held at a negative voltage. The voltage required was initially around −1 V but, over the course of one year, became more strongly negative so that ultimately a voltage of around −6 V was necessary. The progression of the required DC voltage over time is shown in figure 8. At the outer trapping sites (as used in first trap array) the trapping-site electrode was wired directly to ground, and so it was not possible to apply non-zero voltages. It may be that the observed deterioration in the ability to trap ions at an outer trapping site (described above) is related to the need for an offset voltage at the inner trapping site described here.

Application of large DC voltages to the circular trap site electrode complicates the minimization of micromotion when the ion is away from the home position. It will therefore be important to minimize or eliminate the cause of this large, increasing, negative voltage. While this experiment is not unique in observing static compensation voltages which drift significantly over time [31–33] the source of the problem in the situation at hand is not currently known. It may have been caused by a build up of calcium deposited from the oven onto the trap electrodes. This problem can be mitigated by better shielding of the trap electrodes from the oven [34] or by use of a separate loading zone [34, 35]. Alternatively the problem may have been due to materials issues in the electrodes, such as the copper of the electrode bulk diffusing through the gold plating [36, 37] or the growth of field-emission tips [38]. These issues could be overcome by a different selection of materials from which to fabricate the trap.

4.2. RF control of ion position

The proposed implementation of tuning the coherent quantum coupling between separate wells requires that the distance between ions in neighbouring traps can be reduced in an addressable way [15]. In a 2D array of spherical Paul traps this can be achieved by reducing the power applied to individually adjustable RF electrodes between the traps.

Figure 9(a) shows the setup for demonstrating RF control of the ion's position. To move an ion away from the home position in the y direction, the power applied to the y adjustable RF electrode was reduced. Figure 9(b) shows the ion's displacement from the home position as a function of the RF power applied: overall, the ion was displaced by 37 μm for a 5 dB reduction in RF power. For these measurements the phases of the five RF resonators were not locked. As the cooling laser was perpendicular to the displacement direction, any micromotion due to differences in the RF drives' phases would not interfere with laser cooling. Nonetheless, when away from the home position the cooled-ion lifetime was only a few seconds. This may have been due to a reduction in the cooling power as the ion was displaced, given that the cooling-beam diameter was only 40 μm.

The position of the ion in the x direction was varied using a second, adjustable, phase-locked RF drive, applied to the x adjustable electrode. Again, the ion could be displaced ~40 μm by reducing the applied RF power by ~5 dB on the relevant electrode. For this measurement the resonator was phase locked in order to minimize micromotion along the direction of the cooling beam. Used in combination, the two adjustable drive circuits—one on each of the x and y adjustable electrodes—allowed the ion to be moved 'around a corner' in the trap array.

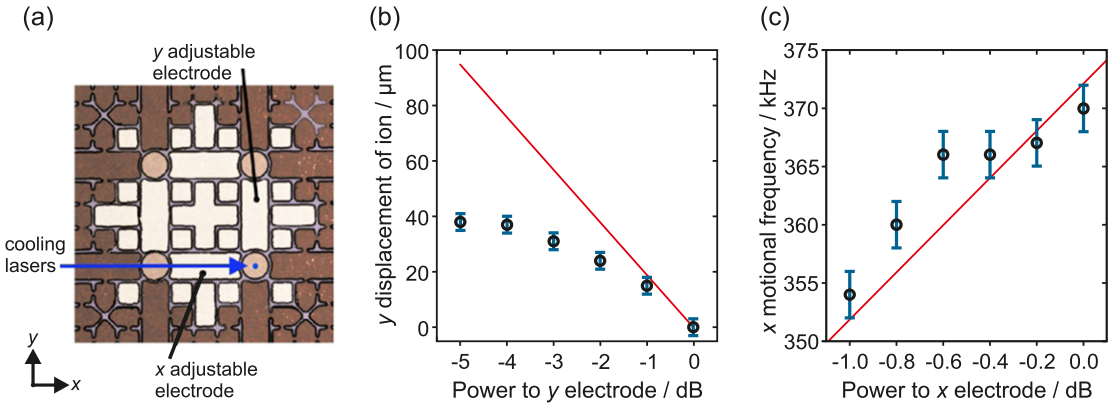

Figure 9. Results of varying the power applied to the adjustable electrodes. (a) Configuration of the laser-cooling and electrode adjustment. The blue dot marks the ion's home position. (b) Points show the displacement of the ion from the home position as a function of the RF power applied to the *y* electrode. The line shows the simulated position of the RF null. (c) Points show the measured motional frequency of the ion as a function of the RF power applied to the *x* electrode. The line shows the simulated change in motional frequency.

4.3. RF tuning of the motional frequency

In addition to reducing the inter-ion spacing, the interaction between ions neighbouring traps can be increased by lowering their motional frequency (see equation (1)). As with the reduction of the inter-ion spacing, this can be achieved by reducing the power applied to the relevant adjustable electrode.

Figure 9(a) shows the setup for demonstrating RF control of the ion's frequency. To reduce the motional frequency in the *x* direction, the power applied to the *x* adjustable RF electrode was reduced. Figure 9(c) shows the ion's motional frequency as a function of the RF power applied: overall, the motional frequency was reduced by 15 kHz for a 1 dB reduction in RF power. For these measurements the adjustable RF resonator was phase-locked to the other resonators so that the variation of the RF voltage did not induce excess micromotion.

The reduction of the applied RF power in the instance shown (as well as the concomitant reduction in the ion's motional frequency) was rather modest. This was because the degradation of the trap behaviour precluded stable trapping for lower RF powers. Operation of the trap at earlier times (with less-severe degradation) demonstrated that stable trapping with applied powers as low as −6 dB is possible (see figure 9(b)). Simulations show that this would correspond to a 25% reduction in the ions' motional frequency. The limited range of the power adjustment is therefore related to a materials issue of the PCB trap; it is not a limitation of the electronics being demonstrated here, nor is it inherent to the scheme of addressing considered.

4.4. Heating rate

The coherent exchange of quantum information between wells in the Cirac–Zoller and the Bermudez schemes motivating this work takes place via the ions' quantized motion. High-fidelity operations require that the ions' motional states are not perturbed by electric-field fluctuations during the time of the gate operation. Such disturbances of the ions' motion are characterized by the ion heating rate, the causes of which are many and varied [39]. The heating rates in the current system were measured at two trapping sites: the outer trapping site used in the first trap array, and the inner trapping site used in the second trap array.

At the outer trapping site the heating rate was estimated by an ion-loss method: A single ion was trapped, and the cooling lasers were turned off for increasing lengths of time. For a 5 s waiting time the ion-loss probability was ∼50%. For the stated operating parameters, simulations give a trap depth of ∼0.1 eV. By calculating the expected loss-rate from a harmonic trap of this depth for a given (constant) heating rate, assuming a thermal distribution of the ion's motion, a heating rate of ∼200 K s^{-1} was inferred. In reality the heating rate is likely to increase as the ion becomes hotter, due to the effect of trap anharmonicities far from the trap centre. Additionally, the stated result assumes that the initial ion temperature was much less than the final temperature, which may not have been the case as the ion was not well cooled in the *z* direction. Consequently the inferred heating rate at this site should be taken as an upper limit of the heating behaviour for cold ions in this trap.

To obtain a more accurate result at the inner trapping site in the second trap array tested, the fluorescence recooling method [40] was used to measure the heating rate. The measurements were performed around one year after the trap had first been installed (see figure 8), by which time the trap behaviour had significantly degraded from its initial condition. Consequently, the uncooled lifetime of ions at this point was only ∼100 ms, compared to ∼1 s in the first trap array.

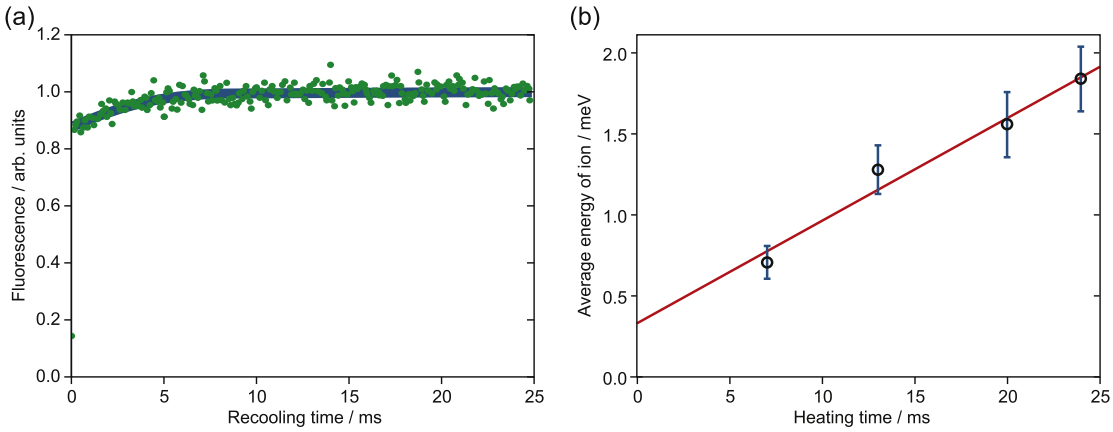

Figure 10. Heating-rate measurement using the recooling method. (a) Fluorescence rate as a function of recooling time (point data, showing an average of 1000 experimental runs) and the recooling-model fit (solid line), after allowing the ion to heat for 24 ms. (b) Energy of the ion, given by the recooling model, as a function of the heating time. A linear fit (solid line) gives a heating rate of 60 ± 20 meV s^{-1}.

For the heating-rate measurements at the inner trapping site, single $^{40}Ca^{+}$ ions were loaded by setting all DC voltages (including DC biases on RF electrodes) to zero, except for the relevant trapping-site electrode which, in this instance, was required to be at −5.3 V. This large negative voltage increased the ion's radial motional frequency to 630 kHz, but reduced its axial frequency to ∼50 kHz. This was a significant perturbation given that, in the absence of DC biases, the radial motional frequency of a spherical Paul trap is half the axial frequency. The ion was Doppler cooled by a laser beam oriented as shown in figure 9(a), which had a slight angle (∼6°) to the plane of the trap surface in order to cool the axial motion. The cooling laser was then turned off for a certain time, during which the uncooled ion was allowed to heat up. Because the axial frequency was so low compared to the radial frequency, it is assumed that predominantly the axial motion was heated [39]. Following a given 'heating time' the ion was re-illuminated by Doppler-cooling light. The motional state of the ion at the end of the heating time was inferred by analysing time-resolved measurements of the fluorescence dynamics as the ion was recooled [40]. Figure 10(a) shows the fluorescence rate during recooling of an ion after it was allowed to heat for 24 ms. For these measurements the 397 nm cooling laser was red-detuned by 10–20 MHz from the centre of the transition, which has a natural linewidth of 21 MHz. The saturation parameter calculated from the measured laser intensity and the linewidth of the effective two-level system was $s = 10 \pm 2$. Similar measurements were carried out for different heating times, shown in figure 10(b). Fitting these points with a line gives a heating rate of (60 ± 20) meV s^{-1}. This corresponds to (700 ± 200) K s^{-1}, and is consistent with the short uncooled ion lifetime observed of ∼100 ms. The level of electric-field noise required to cause such heating is around 10^{-7} V^2 m^{-2} Hz [39].

The level of electric-field noise observed in this trap is high, but not unprecedented [41]. The high heating rate does not appear to be caused by the operation of multiple RF electrodes, since the heating rate is also high with only a single RF drive. We conjecture that the high heating rate may be related to the materials used to fabricate the trap, namely gold-plated copper on a PCB substrate. This work provides the first published heating rate in such a trap. This result, along with experience of other copper-on-PCB traps [42] suggests to us that PCB technologies may not be conducive to the production of traps with low heating rates. In light of these considerations, the heating rate—while problematic in this instance—does not appear to be a limitation inherent to the 2D array architecture or to techniques using variable RF.

5. Outlook and summary

This paper has considered the technological building blocks required to create a 2D array of ion traps in which pairwise interactions between nearest-neighbouring ion traps can be addressably turned on and off. At a single trapping site within a 2D array of ion traps we have demonstrated that an ion's position (in 2D) and its motional frequency can be controllably varied in real time by varying the RF voltage amplitude applied to specific segmented electrodes, while keeping all RF frequencies and phases locked.

Physically interesting systems can be simulated on relatively small arrays, totalling only a few tens of qubits [8, 43]. Section 5.1 discusses the possibilities for miniaturizing the system, so that the distances and frequencies

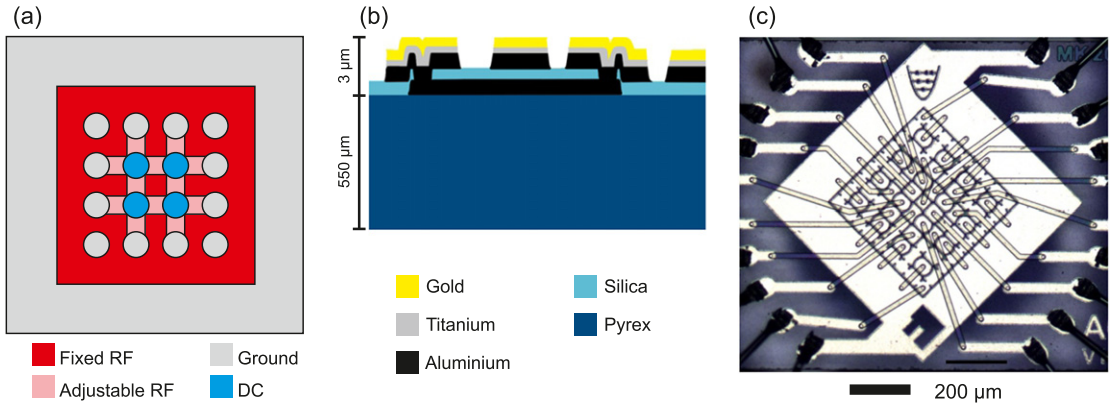

Figure 11. Miniaturized trap arrays. (a) Schematic of a simple array design. This requires multi-layer fabrication processes (b) to connect the 'island' trap electrodes to the bond pads at the edges of the array. (c) Prototype trap currently under test.

involved are commensurate with demonstrating coherent quantum interactions. Section 5.2 considers the prospects for scaling the trap structures, optics and driving electronics to an array of order 10×10 ions.

5.1. Miniaturization

In order for ions in separate harmonic traps to coherently exchange quantum motion, it is desirable to achieve well separations of $\lesssim$100 μm [11, 15]. The PCB prototyping methods used for Folsom are relatively simple at the present scale. However, the minimum possible feature sizes are limited to $\gtrsim$50 μm, which limits the inter-well spacing to $\gtrsim$200 μm. Consequently, even if the other technical issues reported here (specifically, the high heating rate and uncontrolled micromotion) could be solved, PCB technology could not be used to produce a viable 2D array of ion traps for quantum information processing. The limitations of PCB technology do not, however, rule out the possibility of realizing a miniaturized architecture using different materials.

A simple electrode geometry (shown in figure 11(a)) can be considered in which the distance between the trapped ions in their home positions is 100 μm, and for which the ions are 50 μm above the surface. Simulations show that a trap drive with a voltage amplitude of 150 V and a frequency of 100 MHz would give a secular motional frequency of 10 MHz and a trapping-potential depth of 0.1 eV.

By reducing the voltage on the shared adjustable electrode by 10 dB, the inter-ion distance is reduced to 30 μm, while the ions' motional frequency is reduced to 3 MHz. The potential barrier between the wells is only a few meV, though this does not increase the chances of ion loss, since the ions are still confined in the overall 2D array with a deep potential of about 0.1 eV. Under these conditions, the expected gate time is $T_{\text{gate}} \approx 24$ μs (see equation (1)). This gate time compares favourably to the heating rate which may reasonably be achievable in a trap of this size—with care and at cryogenic temperatures—of a few phonons per second [39].

The size scales and parameter ranges outlined above are within reach of current fabrication methods [44]. Fabrication efforts to realize a 2D array of ion traps which is at a scale suitable for quantum information processing are currently underway. The traps are fabricated from aluminium on Pyrex with a gold/titanium surface coating (shown in figure 11(b)). Prototype trap arrays (shown in figure 11(c)) are currently under test.

5.2. Larger numbers of qubits

The complexity of the electrode layout and driving electronics increases linearly with the number of trapping sites: the basic designs shown in figures 9(a) and 4 can simply be replicated many times over. A square array of $N \times N$ ions requires $\sim 2N^2$ independent RF voltage sources. For $N = 10$ this is possible using the same surface-mount components as were used for the present work. Alternatively, integrated electronic components may be used [44] allowing significant miniaturization of a number of components. At room temperature and at trap-drive frequencies of 100 MHz it is not trivial to reduce the physical size of the inductors in the resonators. The use of higher drive frequencies allows smaller inductors to be used. Also operation at cryogenic temperatures allows the possibility of using very much smaller kinetic inductors [45].

As larger arrays are used, a more involved optical setup will be required. To cool the ions it would be useful to have a laser beam broad enough (in the x direction) to cool all ions simultaneously, while being sufficiently tightly focused (in the z direction) to not significantly illuminate (and thereby cause charging of) the trap electrodes. A highly elliptical light sheet which is $\sim$1 mm in one direction, while being focused to a waist of $w_0 \approx 10\mu$m in the other can be achieved for all relevant wavelengths for Ca^+ ions using standard optics.

5.3. Summary

2D arrays of ions in which interactions can be individually addressed constitute an attractive architecture for trapped-ion quantum computing. We have demonstrated the operation of 2D arrays of surface-electrode point ion traps in which the power supplied to specific RF-electrode segments can be varied, while keeping the phase, frequency and all other RF-voltage amplitudes constant. By this means we have demonstrated that an ion's position can be changed and its motional frequency tuned in two-dimensions. This lays the foundations for addressable, tunable, nearest-neighbour interactions between trapped ions in a 2D array.

Acknowledgments

The miniaturized trap array shown in figure 11, and dubbed '*Ziegelstadl*', was fabricated by S Partel in the research group of Prof Edlinger, Fachhochschule Vorarlberg, Dornbirn. This work was supported by the European Research Council (ERC) through the Advanced Research Project CRYTERION and the Proof of Concept Project CARAT; the Austrian Science Fund (FWF) project Q-SAIL; and the Institute for Quantum Information GmbH.

References

[1] Blatt R and Roos C F 2012 Quantum simulations with trapped ions *Nat. Phys.* **8** 277–84
[2] Monroe C and Kim J 2013 Scaling the ion trap quantum processor *Science* **339** 1164–9
[3] Lin G-D, Zhu S-L, Islam R, Kim K, Chang M-S, Korenblit S, Monroe C and Duan L-M 2009 Large-scale quantum computation in an anharmonic linear ion trap *Europhys. Lett.* **86** 60004
[4] Kielpinski D, Monroe C and Wineland D J 2002 Architecture for a large-scale ion-trap quantum computer *Nature* **417** 709
[5] Cirac J I and Zoller P 2000 A scalable quantum computer with ions in an array of microtraps *Nature* **404** 579
[6] Bermudez A, Schmidt P O, Plenio M B and Retzker A 2012 Robust trapped-ion quantum logic gates by continuous dynamical decoupling *Phys. Rev.* A **85** 040302
[7] Hauke P 2013 Quantum disorder in the spatially completely anisotropic triangular lattice *Phys. Rev.* B **87** 014415
[8] Shi T and Cirac J I 2013 Topological phenomena in trapped-ion systems *Phys. Rev.* A **87** 013606
[9] Briegel H J, Browne D E, Dür W, Raussendorf R and Van den Nest M 2009 Measurement-based quantum computation *Nat. Phys.* **5** 19–26
[10] Nigg D, Müller M, Martinez E A, Schindler P, Hennrich M, Monz T, Martin-Delgado M A and Blatt R 2014 Quantum computations on a topologically encoded qubit *Science* **345** 302
[11] Wilson A C, Colombe Y, Brown K R, Knill E, Leibfried D and Wineland D J 2014 Tunable spin–spin interactions and entanglement of ions in separate potential wells *Nature* **512** 57–60
[12] Harlander M, Lechner R, Brownnutt M, Blatt R and Hänsel W 2011 Trapped-ion antennae for the transmission of quantum information *Nature* **471** 200
[13] Brown K R, Ospelkaus C, Colombe Y, Wilson A, Leibfried D and Wineland D J 2011 Coupled quantized mechanical oscillators *Nature* **471** 196
[14] Blakestad R B, Ospelkaus C, VanDevender A P, Wesenberg J H, Biercuk M J, Leibfried D and Wineland D J 2011 Near-ground-state transport of trapped-ion qubits through a multidimensional array *Phys. Rev.* A **84** 032314
[15] Kumph M, Brownnutt M and Blatt R 2011 Two-dimensional arrays of radio-frequency ion traps with addressable interactions *New J. Phys.* **13** 073043
[16] Clark R J, Lin T, Brown K R and Chuang I L 2009 A two-dimensional lattice ion trap for quantum simulation *J. Appl. Phys.* **105** 013114
[17] Sterling R C, Rattanasonti H, Weidt S, Lake K, Webster S C, Kraft M and Hensinger W K 2014 Two-dimensional ion trap lattice on a microchip *Nat. Commun.* **5** 4637
[18] Chiaverini J and Lybarger W E 2008 Laserless trapped-ion quantum simulations without spontaneous scattering using microtrap arrays *Phys. Rev.* A **77** 022324
[19] Lybarger W E 2010 Enabling coherent control of trapped ions with economical multi-laser frequency stabilization technology *PhD Thesis* University of California Los Angeles
[20] VanDevender A P, Colombe Y, Amini J, Leibfried D and Wineland D J 2010 Efficient fiber optic detection of trapped ion fluorescence *Phys. Rev. Lett.* **105** 023001
[21] Herskind P F, Dantan A, Albert M, Marler J P and Drewsen M 2009 Positioning of the RF potential minimum line of a linear Paul trap with micrometer precision *J. Phys.* B **42** 154008
[22] Kim T H, Herskind P F, Kim T, Kim J and Chuang I L 2010 Surface-electrode point Paul trap *Phys. Rev.* A **82** 043412
[23] Tanaka U, Suzuki K, Ibaraki Y and Urabe S 2014 Design of a surface electrode trap for parallel ion strings *J. Phys.* B **47** 035301
[24] Pearson C E, Leibrandt D R, Bakr W S, Mallard W J, Brown K R and Chuang I L 2006 Experimental investigation of planar ion traps *Phys. Rev.* A **73** 032307
[25] Brown K R, Clark R J, Labaziewicz J, Richerme P, Leibrandt D R and Chuang I L 2007 Loading and characterization of a printed-circuit-board atomic ion trap *Phys. Rev.* A **75** 015401
[26] Urabe S, Watanabe M, Imajo H and Hayasaka K 1992 Laser cooling of trapped Ca^{+} and measurement of the $3^{2}D_{5/2}$ state lifetime *Opt. Lett.* **17** 1140
[27] Berkeland D, Miller J, Bergquist J C, Itano W and Wineland D J 1998 Minimization of ion micromotion in a Paul trap *J. Appl. Phys.* **83** 5025
[28] Kumph M 2015 2D arrays of ion traps for large scale integration of quantum information processors *PhD Thesis* Universität Innsbruck
[29] Cetina M, Grier A, Campbell J, Chuang I L and Vuletić V 2007 Bright source of cold ions for surface-electrode traps *Phys. Rev.* A **76** 041401
[30] Home J P and Steane A M 2006 Electrode configurations for fast separation of trapped ions *Quantum Inf. Comput.* **6** 289

[31] Brownnutt M, Letchumanan V, Wilpers G, Thompson R C, Gill P and Sinclair A G 2007 Controlled photoionization loading of $^{88}Sr^{+}$ for precision ion-trap experiments *Appl. Phys.* B **87** 411
[32] Härter A, Krükow A, Brunner A and Hecker Denschlag J 2014 Long-term drifts of stray electric fields in a Paul trap *Appl. Phys.* B **114** 275–81
[33] Narayanan S, Daniilidis N, Möller S A, Clark R, Ziesel F, Singer K, Schmidt-Kaler F and Häffner H 2011 Electric field compensation and sensing with a single ion in a planar trap *J. Appl. Phys.* **110** 114909
[34] Britton J, Leibfried D, Beall J A, Blakestad R B, Wesenberg J H and Wineland D J 2009 Scalable arrays of RF Paul traps in degenerate Si *Appl. Phys. Lett.* **95** 173102
[35] Blakestad R B, Ospelkaus C, VanDevender A P, Amini J M, Britton J, Leibfried D and Wineland D J 2009 High-fidelity transport of trapped-ion qubits through an X-junction trap array *Phys. Rev. Lett.* **102** 153002
[36] Pinnel M R and Bennett J E 1972 Mass diffusion in polycrystalline copper/electroplated gold planar couples *Metall. Trans.* **3** 1989–97
[37] Tompkins H G and Pinnel M R 1976 Low-temperature diffusion of copper through gold *J. Appl. Phys.* **47** 3804–12
[38] Steinhauer S, Brunet E, Maier T, Mutinati G C, Köck A, Schubert W D, Edtmaier C, Gspan C and Grogger W 2011 Synthesis of high-aspect-ratio CuO nanowires for conductometric gas sensing *Proc. Eng.* **25** 1477–80
[39] Brownnutt M, Kumph M, Rabl P and Blatt R 2015 Ion-trap measurements of electric-field noise near surfaces *Rev. Mod. Phys.* **87** 1419
[40] Wesenberg J H *et al* 2007 Fluorescence during Doppler cooling of a single trapped atom *Phys. Rev.* A **76** 053416
[41] Labaziewicz J, Ge Y, Antohi P, Leibrandt D R, Brown K R and Chuang I L 2008 Suppression of heating rates in cryogenic surface-electrode ion traps *Phys. Rev. Lett.* **100** 013001
[42] Splatt F, Harlander M, Brownnutt M, Zähringer F, Blatt R and Hänsel W 2009 Deterministic reordering of $^{40}Ca^{+}$ ions in a linear segmented Paul trap *New J. Phys.* **11** 103008
[43] Nielsen A E B, Sierra G and Cirac J I 2013 Local models of fractional quantum Hall states in lattices and physical implementation *Nat. Commun.* **4** 2864
[44] Guise N D *et al* 2015 Ball-grid array architecture for microfabricated ion traps *J. Appl. Phys.* **117** 174901
[45] Meservey R and Tedrow P M 1969 Measurements of the kinetic inductance of superconducting linear structures *J. Appl. Phys.* **40** 2028–34